Fractal polymer islands on top of ferromagnetic $La_2Ni_{0.6}Mn_{1.4}O_6$ thin films

M. Bernal-Salamanca [a], Z. Konstantinović [b,*], Ll. Balcells [a], M. Šćepanović [b], S. Valencia [c], E. Pannunzio-Miner [d], C. Frontera [a], A. Pomar [a], B. Martínez [a]

[a] Institut de Ciencia de Materials de Barcelona, ICMAB-CSIC, Campus UAB, 08193 Bellaterra, Spain [b] Center for Solid State Physics and New Materials, Institute of Physics Belgrade, University of Belgrade, Serbia [c] Helmholtz-Zentrum Berlin für Materialien und Energie, Albert-Einstein-Str. 15, 12489 Berlin, Germany [d] Facultad de Ciencias Exactas, Físicas y Naturales, Centro de Investigaciones en Ciencias de la Tierra, Av. Velez Sarfield 1611, Ciudad Universitaria, Cordoba, Argentina

ARTICLEINFO

Keywords:
Organic-inorganic materials
Fractal
Poly(ethylene)
Ferromagnetic properties

ABSTRACT

The formation of the crystalline organic polymer (OP) islands on top of double perovskite ferromagnetic $La_2Ni_{1-x}Mn_{1+x}O_6$ (x = 0.4) thin films by RF sputtering is reported. The presence of randomly ramified organic polymer islands for film grown on top of $SrTiO_3$ and $LaAlO_3$ substrates suggest the fractal growth. The stability of fractal OP islands is tested by an in-situ oxygen annealing process as function of the annealing temperature. The evolution of the fractal structure of OP islands is followed in parallel with the evolution of structural and magnetic properties of LNMO thin films. The modification of the manganese valence state due to the presence of organic polymer fractals is studied by means of X-ray photoemission microscopy.

1. Introduction

Hybrid organic–inorganic materials had become a very hot research topic in last years, allowing envisaging new functionalities for many applications (from photovoltaic to field-effect transistors) not achievable within more traditional concepts [1,2]. Among the broad family of organic materials with potential interesting properties, synthetic polymer thin films are good candidates given their wide spectrum of functional properties (from optical to mechanical and electrical) and their extensive range of applications [3]. Polyethylene, the simplest polymer that forms a crystalline structure, is of particular interest due to economic, scientific and life-cycle reasons [4,5]. On the other hand, among inorganic materials double perovskite structure allows a huge structural and compositional flexibility, opening a broad playground for many different applications [6–8].

The structure and physical properties of polymers depend crucially on the crystallization process [4]. The kinetic growth conditions (far from equilibrium) are one of the essential factors to obtain a fractal growth geometry, which enables the exploitation of the recurrence of patterns at increasingly small scales in diverse technologies [9]. As the final performances of polymer-based devices depend crucially of resulting patterns, the understanding of the development of morphological instabilities in ultra-thin polymer films and the surface diffusion on a rigid substrate is of the paramount importance. In this sense, it is worth noticing that vacuum preparation methods allow obtaining fractal growth conditions without the influence of solvent molecules typically present in liquid phase methods [10].

In the present work we report on the formation of the crystalline polyethylene islands on top of double perovskite ferromagnetic $La_2Ni_{1-x}Mn_{1+x}O_6$ (x = 0.4) thin films by RF sputtering, a vacuum- deposition method. The presence of randomly ramified organic polymer (OP) islands suggests the formation of a fractal structure independently of the subjacent substrate ($SrTiO_3$, $LaAlO_3$). Thin film surface properties and stability of OP fractals are studied by X-ray photoemission microscopy in samples with different annealing processes at several temperatures (800–900 °C) and oxygen partial pressure (P_{O2} = 420 Torr).

2. Materials and methods

Thin films growth and characterization: A series of nanostructured organic polymer/$La_2Ni_{0.57}Mn_{1.43}O_6$ (OP/LNMO) heterostructures were grown by RF sputtering under oxygen partial pressure of P_{O2} = 140 mTorr and high temperatures (temperature of the substrate in the range of 800–900 °C) from a nanocomposite organic/La_2NiMnO_6 target. $SrTiO_3$ (STO) and LaAlO3 (LAO) substrates (commercially purchased from CrysTec GmbH) were used for the epitaxial growth of oxide perovskite systems as they present similar crystallographic characteristics as LNMO thin films. As-grown samples were annealed in- situ for 1 h under high oxygen partial pressure (420 Torr) to optimize the magnetic properties of LNMO thin films.

Surface morphology of OP islands was characterized by Scanning Electron Microscopy (SEM), using a QUANTA FEI 200 FEG-ESEM microscope. Atomic Force Microscopy (AFM), (MFP-3D84 AFM from Asylum Research) in taping mode was also used. Structural properties of underlying LNMO thin films were characterized by Reciprocal Space Maps (RSM) using a X'Pert MRD-Panalytical diffractometer. The thickness of the LNMO thin films was determined by reflectivity technique using a Siemens D5000 diffractometer. Magnetic measurements were realized using a Superconducting Quantum Interferometer Device (SQUID, Quantum Design).

Raman scattering measurements were performed at room temperature using a TriVista 557 Raman spectrometer in backscattering micro- Raman configuration with a 300/300/500 groves/mm diffraction gratings combination. A Coherent VerdiG solid state laser with a wavelength of λ =532 nm was used as an excitation source. Laser beam focusing was accomplished by a microscope objective with 100 × magnification and numerical aperture *NA* =0.90. The theoretical diffraction limited spatial resolution is defined by the equation: *Spatial resolution* = 0.61 λ / *NA*, which would predict a spatial resolution of 361 nm in our case. However, typical Raman spatial resolution is often quoted as being in the order of 1 μm, whereas with 'good' samples spatial resolution approaching the diffraction limit can be achieved. The laser power at the sample surface was varied from<1 to 5 mW (the output laser power between 20 and 100 mW). Low laser powers, applied during the collection of Raman spectra of dendritic structures formed at the LNMO/ LAO film surface, was carefully chosen to avoid photochemical or thermal decomposition of these nanostructures.

Space-resolved spectroscopic characterization was done by means of X-ray photoemission electron microscopy (X-PEEM). Experiments were performed at the UE49PGM beam line of BESSY II [11], the synchrotron radiation source of the Helmholtz-Zentrum Berlin, Germany. Data acquisition took place at room temperature. X-PEEM images were recorded for incoming photon energies across the Mn $L_{2,3}$-edge (0.2 eV step size) with linearly polarized radiation. All images were normalized to a background image and drift corrected.

Target preparation: Metal nitrides were dissolved in a 1 M solution of citric acid, in a 6:1 citrate-metal ratio (twice the necessary amount to completely complex the cations). Solutions were heated and stirred until gel formation. Heating proceeded until combustion and dehydration was complete. The resulting brownish ashes were calcined in two stages of 6 h each, first at 300 °C, followed by another cycle at 600 °C for 12 h. The heating rate was 5°Cmin^{-1}. The resulting materials were examined using X-ray diffraction, which

* Corresponding author.
E-mail address: zorica.konstantinovic@ipb.ac.rs (Z. Konstantinović).

confirmed that they have a perovskite structure with no additional phases present, albeit the coexistence of more than one perovskite-like oxides with very similar unit-cell parameters cannot be fully discarded. Although the resulting oxides have a perovskite structure, there are no evidences of cationic order. The powder was then ground with a few drops of of 4% polyvinyl alcohol (PVA) solution as binder, and pressed into circular pellets of 1 in. of diameter. The pellets were sintered twice (two cycles of 6 h at 1350 °C) under argon atmosphere, in order to develop ferromagnetism, with an intermediate grinding.

3. Results and discussion

Fig. 1 shows the formation of nanostructured islands with dendritic morphologies on top of LNMO thin films growth on $SrTiO_3$ (a) and $LaAlO_3$ (b) substrates. In both cases random ramified islands are observed exhibiting a fractal geometry typically observed in systems with very low edge diffusion. The islands are mostly several nanometers high (see below AFM figure), although we have observed some branches with high up to several tens of nanometers. The fractal dimension (D_f) of fractal islands, evaluated by the box counting method [12], is very similar in both films and is found to be in the

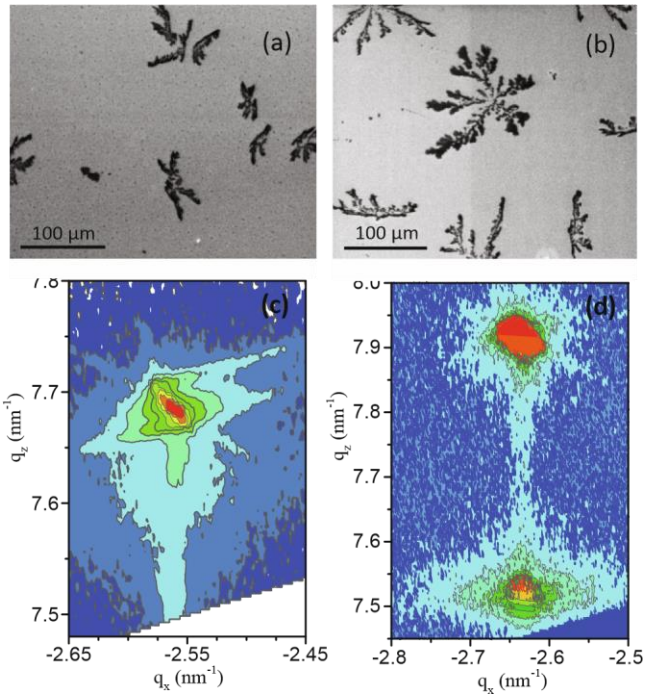

Fig. 1. SEM micrograph of fractal nanoislands on top of $La_2Ni_{0.57}Mn_{1.43}O_6$ grown on the surface of (a) $SrTiO_3$ and (b) $LaAlO_3$ substrate. The panels (c) and (d) show RSM around (103) reflection for the corresponding thin films.

range of $1.5 < D_f < 1.7$ (see below). The fractal dimension of $D_f = 1.62$, evaluated in the case of OP/ LNMO on top of LAO thin films is very close to theoretical estimation of $D_f = 1.72$ in the diffusion limited aggregation (DLA) model with the sticking coefficient of 1, where edge diffusion is not permitted [13,14].

The structural strain of the underlying LNMO thin films grown on top of STO and LAO substrates was analyzed by means of Reciprocal Space Maps (RSM). RSM around (103) reflection of the corresponding thin films (Fig. 1(c)-(d)), evidenced that the underlying 40 nm thick LNMO films are fully strained, as previously reported [8]. The estimated in- plane and out of plane parameters in pseudo cubic perovskite notation are $a_{||}$=3.905 Å and $a_{\perp}$=3.941 Å in LNMO/STO and $a_{||}$=3.789 Å and $a_{\perp}$=3.978 Å in LNMO/LAO thin films, giving rise to LNMO cell parameters a = b = 5.522 Å, c = 7.868 Å and a = b = 5.358 Å, c = 7.956 Å, respectively.

Since X ray diffraction could not detect any additional peak, the composition of fractal-like islands was investigated by Raman spectroscopy (Fig. 2). Fig. 2(a) shows Raman spectra of OP/LNMO thin film on top of LAO, recorded in parallel and crossed polarizations of incident and scattered light. Beside the LAO Raman peaks detected below 500 cm^{-1}, two broad Raman features dominate the parallel-polarized spectrum. The feature located around 598 cm^{-1} could be related to antisymmetric stretching (AS), whereas the feature at about 685 cm^{-1} could be assigned to symmetric stretching (S) vibrations of $(Ni/Mn)O_6$ octahedra characteristic for LNMO structure [15,16,17]. The decomposition of the spectral structure between 500 and 800 cm^{-1} according to the procedure proposed by Iliev et al. [16] reveals Raman bands at about 507, 555, 598, 644, 667 and 689 cm^{-1} (see the inset in Fig. 2a). Note that the frequencies of both AS and S modes of the film are appreciably higher than the corresponding phonon frequencies in the LNMO single crystal [16]. Pronounced blueshifts [14] could be related to compressive stress in the LNMO thin films, due to the lattice mismatch between the film and the substrate (see Fig. 1(d)). Also, significantly higher Mn amount in the film under investigation than in the stoichiometric LNMO could be partly responsible for the observed blueshift of the Raman modes (knowing that the atomic mass of Mn(54.938) is lower than that of Ni (58.693)) [17].

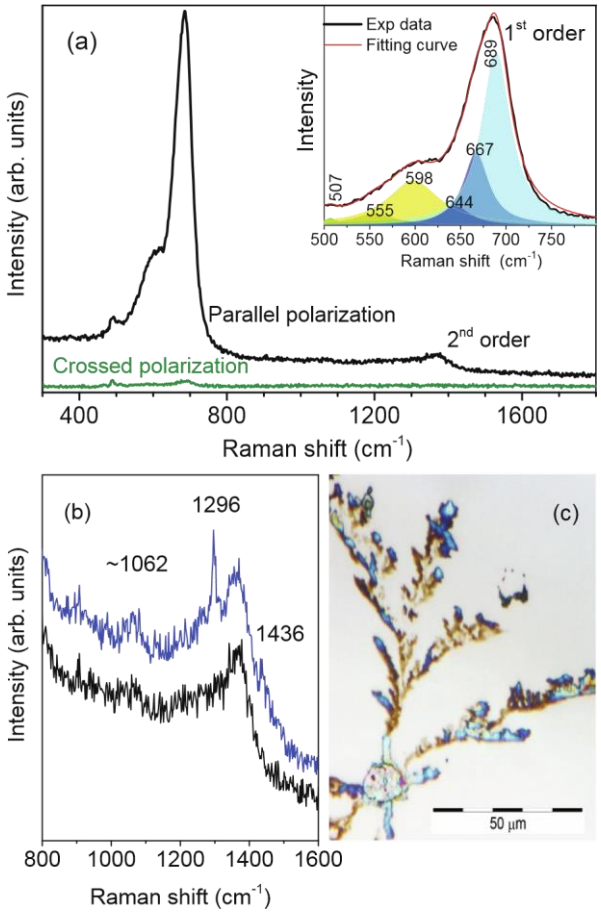

Fig. 2. (a) Polarized Raman spectra of LNMO/LAO thin film at 300 K. Inset shows the fit of the spectral profile obtained in parallel polarization by a sum of Lorentzians ascribed to 1st order LNMO Raman modes. (b) Raman spectra in the range of 800–2000 cm^{-1} measured on blue part of fractal-like island (blue line) and clean film surface (black line). (c) Micrograph of fractal-like islands seen under the 50 × objective of optical microscope coupled to the Raman spectrometer.

To identify the subtle changes between the surface with/without fractal-like island the optical microscope coupled to the Raman spectrometer was used (Fig. 2(c)). It is worth noticing, that these islands are very sensitive to the irradiation by a focused laser beam. Thus, soon after the exposure to the laser

beam (even with a power of<1 mW) brown parts of ramified branches began to fade and disappear, leaving only a clean surface of the film. Only structures of intense blue colour proved to be more resistant to the laser irradiation, which enabled measurement of their Raman spectra. These spectra show some subtle differences above 1000 cm^{-1} in comparison to the spectra recorded on the clean film surfaces, as shown in the Fig. 2(b). Additional peaks detected in the spectra of blue parts of branches at about 1062, 1296 and 1436 cm^{-1} could be related to the C–C symmetric stretching, the CH_2 twisting and CH_2 bending modes, respectively, usually attributed to vibrational bonds of alkyl groups C_nH_{2n+1} [18]. In spite of the low signal-to-noise intensity ratio and the appearance of the LMNO second order mode in the spectral range of interest, the relatively narrow band at about 1296 cm^{-1} may be an indication of the polyethylene rotator (semi- crystalline) or crystalline phases [4].

At first instance, the origin of these organic material seems puzzling. It may look reasonable to expect that any organic material was burnt either during sintering of the oxide target or during the deposition of the film at high temperature. Any possible contamination should be disregarded as film growth occurs in a very controlled atmosphere free of organic material. Thus, the most plausible scenario is to assume that, during target preparation by the citrate decomposition method, a nanocomposite between PVA and oxide (LNMO) was formed that modifies the thermal decomposition of PVA. We should remind that PVA is widely used for binder in ceramic pellets as it is a very good agglutinant that, usually, is later destroyed during the thermal treatment. However, it has been shown that when PVA is part of a nanocomposite, its thermal decomposition may be significantly modified to higher temperatures [19]. In this scenario, organic material remaining from PVA decomposition may remain at the target (forming thus a nanocomposite target PVA/LNMO) and then it is transferred during or at the end of film deposition, forming the observed fractal-like islands.

The stability of fractal-like OP islands was tested by in-situ annealing processes in oxygen right after thin film growth as a function of the annealing temperature. Annealing processes after thin films growth are usually employed to improve ferromagnetic properties in perovskite oxides, ensuring the proper oxygen stoichiometry [20]. The evolution of the fractal structure of islands (Fig. 3) is followed in parallel with the evolution of structural and magnetic properties of LNMO thin films (Fig. 4).

As mentioned above, OP islands in as-grown samples (without additional in-situ annealing) show fractal-like structures with randomly ramified branches. The evaluated fractal dimensions (Fig. 4(a)) in as- grown films are not far away from theoretical value of 1.7 within the simplest DLA scenario [13], suggesting very limited edge diffusion. With an additional annealing process, the form of OP islands progressively turns to compact islands. At the first stage (annealing at 800 °C), the widening of ramified branches is observed (Fig. 3(b)), followed by (annealing at 850 °C) the complete loss of small branches (Fig. 3(c)). After annealing at 900 °C, the OP islands exhibit a compact rounded shape (see Fig. 5(b)). Lateral evaporation cannot be excluded.
Experimental observations can be explained well within the diffusion limited aggregation model with reduced atom-sticking coefficient [13,14]. The reduced value of the sticking coefficient (initial value of s = 1) leads to the widening of ramified branches and to the increase of the fractal dimension of islands [14], in agreement with our estimation shown in Fig. 4(a). Further increase of the annealing temperature leads to the disappearance of small branches of PE fractal islands and the further increase of the fractal dimension, approaching $D_f = 2$ in the case of the rounded shape islands (see below Fig. 5(b)), as expected for two dimensional objects. The reduction of the atom-sticking coefficient could be justified by the lateral evaporation of atoms from islands, expected during annealing at very high temperatures. Within this model, the crossover between fractal-like and compact islands is expected for reduced sticking coefficient value of s = 0.032, i.e. 3.2% of probability that an atom can be stuck at the current position [13,14], which lead to an estimation of the sticking coefficient in the range of $0.03 < s < 0.06$ for $T_{ann} = 850$ °C and below $s < 0.01$ for $T_{ann} = 900$ °C in our case. However, these values should be taken as upper limits as the edge diffusion within DLA scenario is not considered [14] nor the enhanced importance of the lateral evaporation during annealing at high temperatures (850 °C < Tann < 900 °C).

At the same time, as mention before, the structural and magnetic properties improve with the annealing process at the high temperature right after thin film growth. For annealing temperatures in the range 800 °C < T < 900 °C in-plane lattice constant of all the films perfectly matches that of the STO/LAO substrate (red and blue dotted line in Fig. 4 (b)), indicating that films are fully strained. simultaneously, the out-of- plane lattice constant decreases after successive annealing process (left- hand scale at Fig. 4(b)). The decreasing of the out-of-plane lattice parameter after successive annealing processes could be consistent with oxygen incorporation into structure assuring the proper oxygen stoichiometry, as previously reported [20].

The as-grown thin films show reduced magnetic transition temperature ($150\ K < T_c < 180\ K$) compared with the value of double perovskite La_2NiMnO_6 single crystal (T_c(LNMObulk) = 270 K). The structural changes shown above leads, as expected, to an increase of the ferromagnetic transition temperature of the LNMO thin films approaching the bulk-like value for annealing process above $T_{ann} \geq 850$ °C [8] (right- hand scale in Fig. 4(b)).

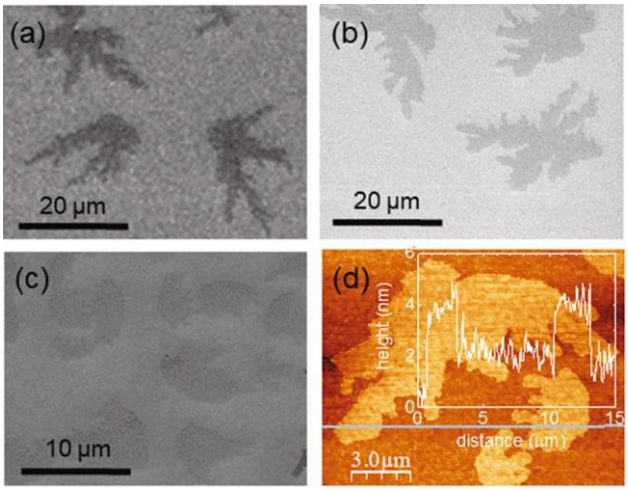

Fig. 3. Evaluation of nano-islands: (a) without annealing process and under oxygen annealing PO_2 = 420 Torr at (b) 800 °C and (c) 850 °C with corresponding AFM image (d). In the inset, the typical profile line.

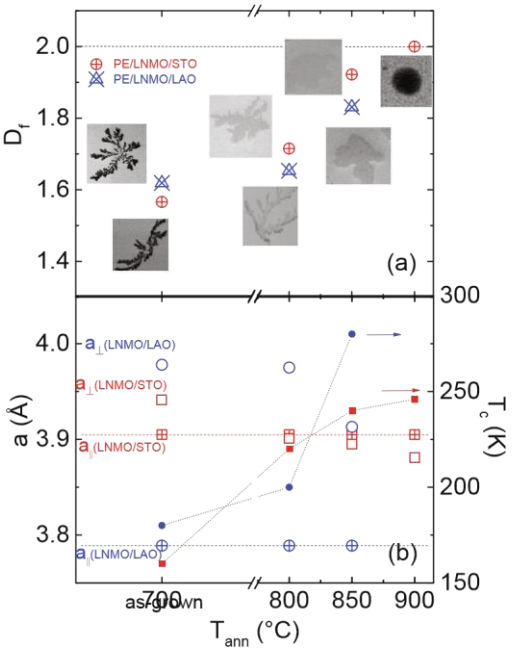

Fig. 4. (a) Variation of fractal dimension of organic polymer nanoislands on top of LNMO thin films under different oxygen annealing process (b) Variation of in-plane and out-of-plane lattice parameters of LNMO thin films with corresponding ferromagnetic transition under different annealing process.

In order to investigate whether the oxidation state of Mn is affected by the presence of PE islands on top of LNMO the space-resolved X-ray absorption spectroscopy (XAS) experiments have been carried out on the OP/LNMO thin films annealed at 800 °C and at 900 °C. As in SEM imaging, OP islands imaged by X-PEEM show a dark contrast as compared to the bright one for LNMO regions with no OP on top (see Fig. 5(a) and 5(b)). Mn L2,3 XAS spectra have been extracted from dark (OP on top of LNMO) and bright (bare LNMO) regions, red and black curves, respectively in Fig. 5(c) and 5(d). Independently of the annealing temperature, we observe notable spectral differences between both curves. Note that the XAS spectra obtained from regions with OP islands present an increase of the spectral weight at the low energy side of the L3 peak, at ca. 640.8 eV, as compared to that of pure LNMO regions.

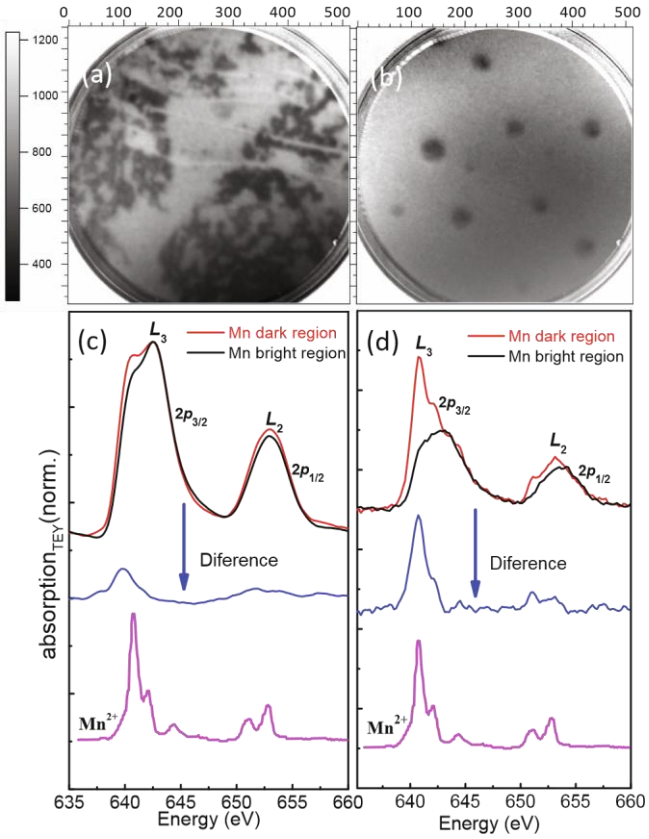

Fig. 5. (a) and (b) X-PEEM images computed from the sum of images obtained across the Mn $L_{2,3}$ edge (0.2 eV step size) for samples annealed under oxygen pressure at (a) T_{ann} = 800 °C and (b) T_{ann} = 900 °C. Field of view 20 um. (c) and (d) Corresponding XAS Mn $L_{2,3}$ spectra obtained from dark (red curve) and bright (black curve) regions for (a) and (b), respectively. Blue curve is obtained as the difference of XAS spectra for dark and bright areas after proper normalization (see text). Magenta curve is a digitalized version of a theoretical Mn^{2+} spectra reported in [22].

In order to reveal the origin of such difference we normalize the spectra following the procedure described in [21] and plot their difference (blue curve in Fig. 5(c) and (d)). In both cases, i.e. for fractal-like (Fig. 5 (a)) and rounded-shape (Fig. 5 (b)) islands, the difference spectrum mimics spectral features typical of divalent Mn [22]. We hypothesize that the presence of carbon in OP is at the heart of the formation of Mn^{2+}in agreement with [23] and leads to the deviation of the nominal mixed Mn^{3+}/Mn^{4+} state, observed previously [8]. The annealing process at high temperatures (T_{ann} = 900 °C), additionally enhances the formation of divalent Mn at the OP/LNMO interface.

4. Conclusion

In conclusion, the nanostructured organic fractal-like islands are prepared on top of ferromagnetic $La_2Ni_{0.57}Mn_{1.43}O_6$ thin films with solvent free RF sputtering. The Raman spectra of ramified islands is consistent with vibrational bonds of alkyl groups C_nH_{2n+1} and the presence of polyethylene phases. The in-situ annealing processes under high oxygen pressure at high temperature improve the ferromagnetic properties keeping thin films in-plane fully strained. The increase of the annealing temperature leads to the crossover from fractal-like phase to compact OP islands, i.e. from fractal dimension towards two- dimensional objects. Finally, the presence of OP islands changes the manganese valence from mixed valence state towards Mn^{2+} states, which anticipates a substantial change of the surface resistance that could be of strong interest for the development of devices.

Author statement

M. Bernal-Salamanca: thin film preparation and characterization, manuscript preparation, Z. Konstantinovi´c and Ll. Ballcels: supervision, manuscript preparation, M. S ´cepanovi´c: Raman measurements, S. Valencia: X-PEEM measurements, E. Pannunzio-Miner: Target preparation, C. Frontera, A. Pomar and B. Martinez: Reviewing and editing manuscript.

Declaration of Competing Interest

The authors declare that they have no known competing financial interests or personal relationships that could have appeared to influence the work reported in this paper.

Acknowledgements

This work has received funding from the European Union's Horizon 2020 research and innovation under the Marie Sklodowska-Curie grant agreement No. 645658 (DAFNEOX Project). A.P. and Z.K. thank Senzor- INFIZ (Serbia) for the cooperation provided during their respective secondments. E. P.-M. acknowledge financial support from the Spanish Ministry of Economy and Competitiveness through the "Severo Ochoa" Programme for Centers of Excellence in R&D (CEX2019-000917-S), and project MAT2015-71664 and SPINCURIOX (RTI2018-099960-B-I00). M. S. and Z. K. acknowledge the support of the Serbian Ministry of Ed ucation, Science and Technological Development (Projects No III45018). This work has been performed in the framework of the PhD program of the Universitat Autonoma de Barcelona (UAB).

References

[1] Y.H. Lee, M. Ha, I. Song, J.H. Lee, Y. Won, S. Lim, H. Ko, J.H. Oh, Hihg- performance hybrid photovoltaics with efficient interfacial contacts between vertically aligned ZnO nanowire arrays and organic semiconductors, ACS Omega 4 (2019) 9996.

[2] F. Maddalena, X.Y. Chin, D. Cortecchia, A. Bruno, C. Soci, Brightness enhancement in pulsed-operated perovskite light-emitting transistors, ACS Appl. Mater. Interfaces 10 (2018) 37316.

[3] I. Melnichuk, A. Choukov, M. Bilek, A. Weiss, M. Vandrocova, L. Bacakova, J. Hanus, J. Kousal, A. Shelemin, P. Solar, D. Slavinska, H. Biederman, Direct covalent coupling of proteins to nanostructured plasma polymers: a route to tunable cell adhesion, Appl. Surf. Sci. 351 (2015) 537.

[4] K.B. Migler, A.P. Kotula, A.R.H. Walker, Trans-rich structures in early stage of crystalization of polyethylene, Macromolecules 48 (2015) 4555.

[5] P.A. Choukourov, P. Pleskunov, D. Nikitin, R. Tafiichuk, A. Shelemin, J. Hanus, J. Majek, M. Ungel, A. Roy, A. Ryabov, Plasma-assisted growth of polyethylene fractal nano-islands on polyethylene oxide films: impact of films confinement and glassy dynamics on fractal morphologies, Appl. Surf. Science 489 (2019) 55.

[6] W.-J. Yin, B. Weng, J. Ge, Q. Sun, Z. Li, Y. Yan, Oxide perovskite, double perovskites and derivatives for electrocatalysis, photocatalysis and photovoltaic, Energy Environ. Sci. 12 (2019) 442.

[7] M.S. Sheikh, D. Ghosh, A. Dutta, S. Bhattacharyya, T.P. Sihna, Lead free double perovkite oxides Ln2NiMnO6 (Ln=La, Eu, Dy, Lu), a new promising material for photovoltaic applications, Mater. Sci. Eng., B 226 (2017) 10.

[8] M. Bernal-Salamanca, Z. Konstantinovic, Ll. Balcells, E. Pannunzio-Miner, F. Sandiumenge, L. Lopez, B. Bozzo., J. Herrero-Martin, A. Pomar, C. Frontera, B. Martinez, Nonstoichiometry driven ferromagnetism in double perovskite La2Ni1- ´ xMn1+xO6 insulating thin films, Crystal Growth and Design 19 (2019) 2765.

[9] M.S. Fairbanks, DNMc Carthy, S A Scott, S A Brown and R P Taylor, Fractal electronic devices: simulation and implementation, Nanotechnology 22 (2011) 365304.

[10] B. Wang, S. Tang, Y. Wang, C. Shen, R. Reiter, G. Teiter, J. Chen, B. Zhan, Systematic control of self-seeding crystallization patterns of poly(ethylene oxide) in thin films, Macromolecules 51 (2018) 1626.

[11] F. Kronast and S. Valencia Molina, J. Large-Scale Res. Facil. 2, A90 (2016)]. [12] www.complexityexplorer.org/courses/93-fractals-and-scaling.

[13] X. Wang, Y. Huang, Calculation of the fractal dimension of diffusion-limited aggregation by the renormalization-group approach in an arbitrary Euclidean dimension, Phys. Rev. A 46 (1992) 5038.

[14] A. Ghosh,1 R. Batabyal, G. P. Das, and B. N. Dev, An extended fractal growth regime in the diffusion limited aggregation including edge diffusion, AIP Adv. 6 (2016) 015301.

[15] H.Z. Guo, J. Burgess, E. Ada, S. Street, A. Gupta, M.N. Iliev, A.J. Kellock, C. Magen, M. Varela, S.J. Pennycook, Influence of defects on structural and magnetic properties of multifunctional La_2NiMnO_6 thin films, Phys. Rev. B 77 (2008), 174423.

[16] M.N. Iliev, M.M. Gospodinov, M.P. Singh, J. Meen, K.D. Truong, P. Fournier, S. Jandl, Growth, magnetic properties and Raman scattering of La_2NiMnO_6 single crystals, J. Appl. Phys. 106 (2009), 023515.

[17] M. Nasir, M. Khan, S. Bhatt, A.K. Bera, M. Furquan, S. Kumar, S.M. Yusuf, N. Patra, D. Bhattacharya, S.N. Jha, S.-W. Liu, S. Biring, S. Sen, Influence of Cation Order and Valence States on Magnetic Ordering in $La_2Ni_{1-x}Mn_{1+x}O_6$, Phys. Status Solidi B 256 (2019) 1900019.

[18] A.P. Kotula, M.W. Meyer, F. De Vito, J. Plog, A.R. Hight Walker, K.B. Migler, The rheo-Raman microscope: Simultaneous chemical, conformational, mechanical, and microstructural measures of soft materials, Rev. Sci. Instrum. 87 (2016), 105105.

[19] P.B. Messersmith, S.I. Stupp, High-Temperature Chemical and Microstructural Transformations of a Nanocomposite Organoceramic, Chem. Mater. 7 (1995) 454.

[20] Z. Konstantinovic, J. Santiso, Ll. Balcells, B. Martínez, Strain driven self-assembled network of antidots in complex oxide thin films, Small 5 (2008) 265.

[21] S. Valencia, A. Gaupp, W. Gudat, Ll. Abad, Ll. Balcells, A. Cavallaro, B. Martínez, F. J. Palomares, Mn valence instability in La2/3Ca1/3MnO3 thin films, Phys Rev B 73 (2006) 104402.

[22] G van der Laan, I W Kirkman, The 2p absorption spectra of 3d transition metal compounds in tetrahedral and octahedral symmetry, J. Phys.: Condens. Matter 4 (16) (1992) 4189–4204.

[23] S. Valencia, A. Gaupp, W. Gudat, Ll. Abad, Ll. Balcells, B. Martínez, Impact of microstructure on the Mn valence of La2/3Ca1/3MnO3 thin films, Phys.Rev. B 75 (2007) 184431.